# Chapter 9

# Swirl Stabilized Flame Study : Experimental Procedure

## 9.1 Turbulent Variable Swirl Combustor Assembly

The turbulent variable swirl combustor described in Chapter 8 was fabricated. The combustor was assembled in a support structure starting with the plenum. The central fuel injection system was inserted from the bottom. The axial air injection tubes were inserted and locked into the four axial ports. The honeycomb and the perforated plate were assembled into the plenum. The fabricated tee was then bolted to the top of the plenum. The centering apparatus used for ensuring the proper centering of the central fuel injection system was inserted into the swirl generation section of the combustor, which then along with the burner head and the combustion chamber back plate was assembled on the top of the tee. The central fuel injection system was then aligned such that the top surface of the center body was 2.5 mm below the entrance of the quarl and the fuel injection ports were about 150 mm upstream of the entrance of the quarl. Using the centering apparatus, the radial location of the center body was changed to ensure that it was perfectly aligned to the central axis of the combustor. The 24 radial fuel injection ports were plugged. The speaker was attached to the side branch of the tee. Care was taken to ensure that there was enough spacing between the speaker mount and the side branch flange for the unhindered movement of the speaker

cone. This was achieved by placing gasketing material between the side branch flange and the speaker mounting flange. Piping for cooling water was plumbed to both the center body and the combustion chamber back plate. The piping network for both the fuel and the air systems, including their flow control and measuring equipments were assembled and connected to their respective ports on the combustor. Fuel was supplied through a bank of 4 to 6 high pressure bottles, while air was supplied by an Ingersoll Rand 150 scfm compressor. Having assembled the rest of the combustor and the piping network, the quartz combustion chamber was assembled on its back plate. The support assembly for the quartz tube at the downstream end was finally put in place. All the contacts between the quartz tube and the metallic surfaces were insulated using Fiberfrax. The 'Type R' thermocouples were inserted into their respective positions in the quartz combustion chamber.

## 9.2 Assembly of the Velocity Probe

Two Radio shack microphones having the same amplitude and the same phase resonance characteristics were selected to build the velocity probe. The frequency response characteristics of the two microphones were tested and were ensured to have their FRF magnitude to be within $\pm 0.5$ dB and the FRF phase between $\pm 0.5$ degrees. Details of the testing procedure are described in Chapter 5, Section 5.2 and the resulting FRF magnitude and the phase characteristics are shown in Figure 9.1 and Figure 9.2 respectively. The two microphones were then fitted into their respective holding tubes and inserted into the ports provided in the burner head. The assembly ensured that the sensing element were flush with the wall of the flow passage within the burner head. Outside the combustor, the wires of both the microphones were soldered separately to an independent 1.5 volt DC power source.

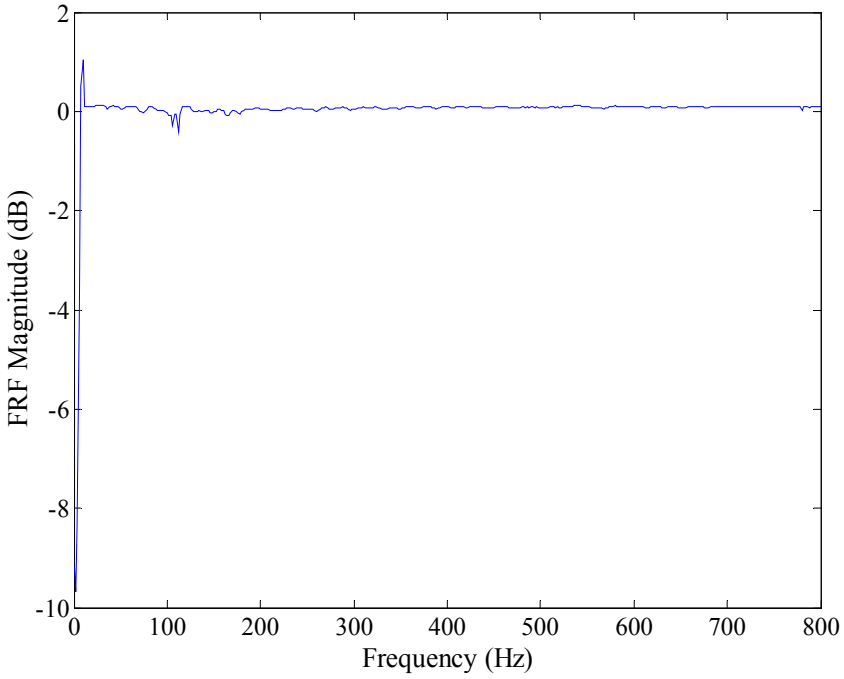


Figure 9.1: FRF (magnitude) of microphone '3' to microphone '4'

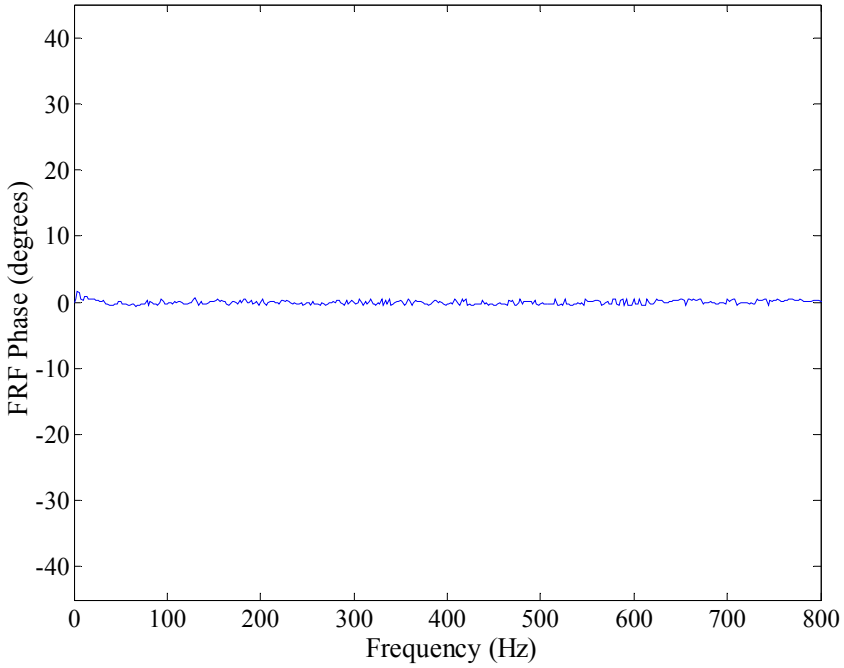


Figure 9.2: FRF (phase) of microphone '3' to microphone '4'

## 9.3 Acoustic Characterization

With the burner assembled and the microphones inserted, acoustic measurements were taken to characterize the frequency resolved acoustic velocity at a plane 45 mm below the entrance of the quarl. The speaker was imparted a white noise signal from the signal generator under no flow conditions. The FRF along with the coherence between the velocity probe signal and the speaker voltage was recorded. The magnitude of the FRF is shown in Figure 9.3, while the coherence between the two signals is shown in Figure 9.4. This exercise was conducted to identify the velocity modes of the burner, and also to determine the frequencies which produce a velocity node at the plane of the measurement.

Figure 9.3 shows the combustor to exhibit acoustic velocity modes at about 25, 190, 270, and 460 Hz. Within the bandwidth of 20-400 Hz, Figure 9.4 shows a coherence greater than 0.85 for the frequency range of 20-140 Hz and 170-400 Hz, with a small dip at 350 and 360 Hz. Between 140 and 170 Hz, the coherence plummets down very sharply and is almost zero at about 160 Hz, indicating the presence of a velocity node at 160 Hz at the plane of the measurement. Thus, while conducting the experiments, close attention needs to be given to the region of 140-170 Hz, so as to maximize the number of acceptable data points by altering the speaker voltage and maintaining a constant level of velocity perturbations at the plane of the measurement. Nevertheless, there is expected to be some loss of dynamic data points around 160 Hz, due to the presence of velocity node at this frequency. Figure 9.3 also shows the magnitude of the FRF between the velocity signal and the input to the speaker for conditions with 25 scfm of flow but no flame, and also for conditions in the presence of a flame. Comparison of the three plots in Figure 9.3 shows that, although the presence of the flow and the flame makes the FRF seem a little more noisy than at the condition with no flow, the dominant acoustic characteristics are preserved. The primary conclusion of the acoustic characterization is that the velocity probe provides an accurate measure of the velocity upstream of the flame within the bandwidth of 20-400 Hz. However, some of the dynamic data around 160 Hz is unreliable and is not used.

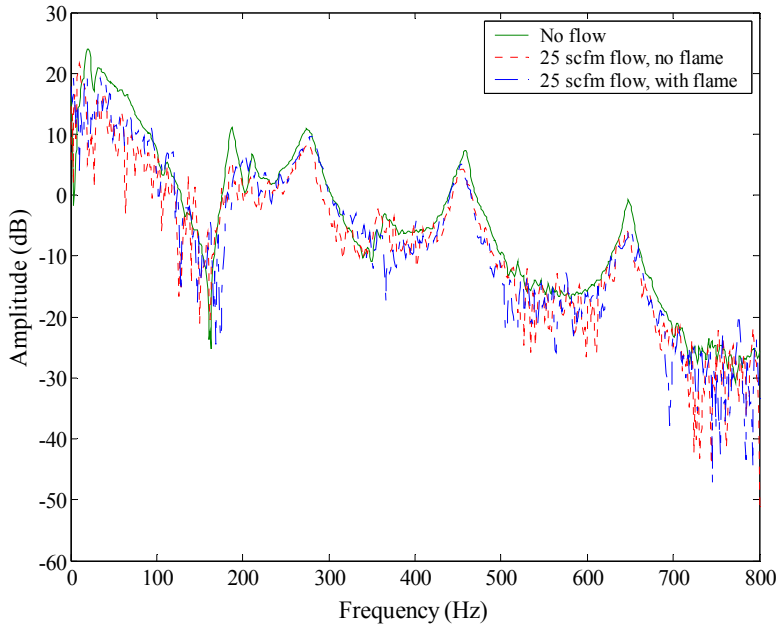


Figure 9.3: FRF (magnitude) of the velocity probe output and the speaker input

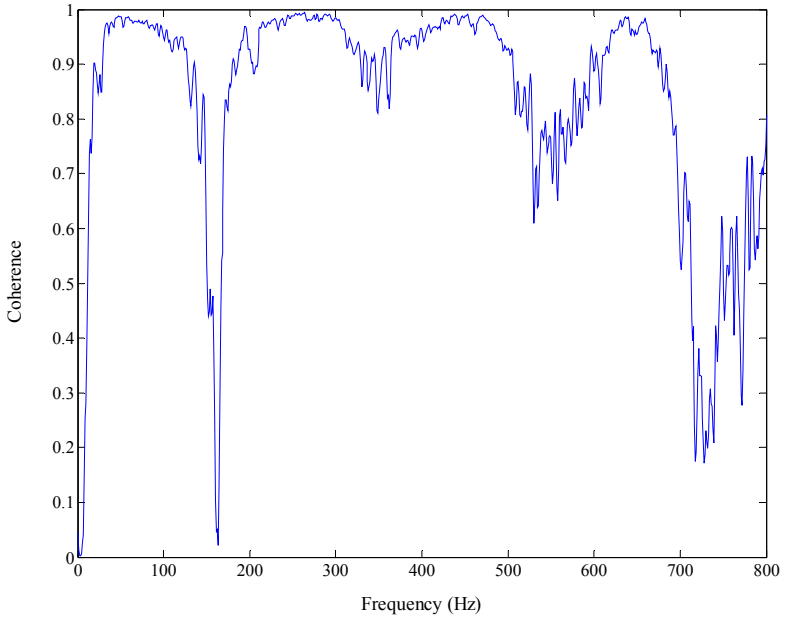


Figure 9.4: Coherence between the velocity probe output and the speaker input

## 9.4 Flow Field Characterization

Swirling flows result from the application of a spiraling motion to the flow. This is normally achieved by imparting tangential velocities to a perfectly axial flow. The degree of swirl imparted has a profound effect on the resulting flow field. Thus, while studying combustion in swirl stabilized flames, the flow field must be characterized and also the swirl strength must be known. The characterization of the flow field is done by measuring the velocity profile across the cross section of flow, while the degree of the swirl (swirl strength) is characterized by a non-dimensional swirl number ($S$), which represents the axial flux of the swirl momentum divided by the axial flux of the axial momentum times the equivalent nozzle radius. Thus,

$$S = \frac{G_\theta}{G_z \frac{d}{2}} \tag{9.1}$$

where

$$G_\theta = \int_0^R (\rho\, u_z\, u_\theta + \rho\, \overline{u_z' u_\theta'})\, r^2\, dr \tag{9.2}$$

is the axial flux of the circumferential momentum that also includes the $x-\theta$ direction of the turbulent shear stress term, and

$$G_z = \int_0^R (\rho\, u_z'^2 + \rho\, \overline{u_z^2} + (p - p_\infty))\, r\, dr \tag{9.3}$$

is the axial flux of the axial momentum including the z direction turbulent stress term and a pressure term representing the axial thrust. Often the characterization of the swirl number given by equations 9.1 to 9.3 is difficult to experimentally measure with a high certainty. Therefore, simplifications to the definition are abundant in literature, and Gupta et al. [80] discuss a number of them. Equations 9.1 to 9.3 were simplified to eliminate the need for static pressure measurement by Ribiero et al. [81]. The final form of the simplification is given by

$$S = \frac{\int_{R_i}^{R_o} \rho\, u_z\, u_\theta\, 2\pi\, r^2\, dr}{\int_{R_i}^{R_o} \rho\, (u_z^2 - \frac{u_\theta^2}{2})\, 2\pi\, R_o\, r\, dr} \tag{9.4}$$

In the present research effort, the velocity profiles are generated using a hotwire, and the swirl number is obtained by using the experimentally generated velocity profiles and equation 9.4.

However, this procedure requires the knowledge of the velocity profiles at every condition where the swirl number needs to be known. This is not the case if the swirl number was characterized using a geometric swirl number, as proposed by Claypole and Syred [82] for swirl generation configurations, similar to the one used in the present study. This geometric swirl number ($S_g$), is defined as

$$S_g = \frac{R_o \, \pi \, r_e}{A_t} \frac{(Tangential\ flow\ rate)^2}{(Total\ flow\ rate)^2} \tag{9.5}$$

where $R_o$ is the radius of the inlet of the quarl, $r_e$ is the radius on which the tangential inlets are attached with respect to the center of the combustor and $A_t$ is the total area of the tangential inlet.

The drawback of using equation 9.5 is the idealized assumption that there is perfect mixing between the axial and the tangential streams, which cannot be achieved in reality. Furthermore, there is a decay in the generated swirl, as the flow moves downstream of the plane of swirl generation. Thus, the actual swirl intensity at the inlet of the quarl is quite different from the one predicted by $S_g$. Therefore, to be able to effectively use $S_g$, a relationship between $S$ and $S_g$ is required. Based on the above discussion, for the present experimental setup, velocity data for 15 different $S_g$ were collected and the corresponding $S$ was evaluated using equation 9.4. The calculated $S$ was found to be equal to $0.26\,S_g$, within a deviation of $\pm 6\%$. Thus, using this calibration, it is possible to deduce $S$ directly from the measurements of the mass flow meters. A similar procedure was also used by Feikema et al. [83].

### 9.4.1 Velocity Measurement

The velocity field was measured under non-reacting conditions at both the inlet of the quarl and the inlet of the dump, as shown in Figure 9.5, using a hotwire anemometer. For the purpose of presentation of this data, '$u_z$' is the direction along the axis of the combustion, while '$v$' and '$w$' are two orthogonal directions that lie on a plane perpendicular to '$u_z$'. Figure 9.6 shows the velocity profiles across the diameter at an axial location of 1.5 mm above the entrance of the dump. Three data sets are plotted, each taken along the diameter

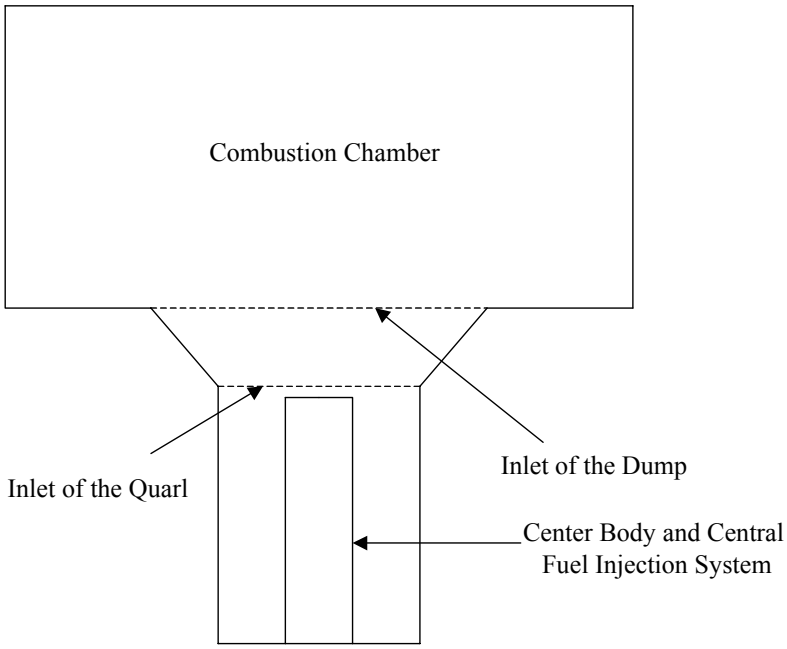


Figure 9.5: Schematic showing the quarl and the dump inlets

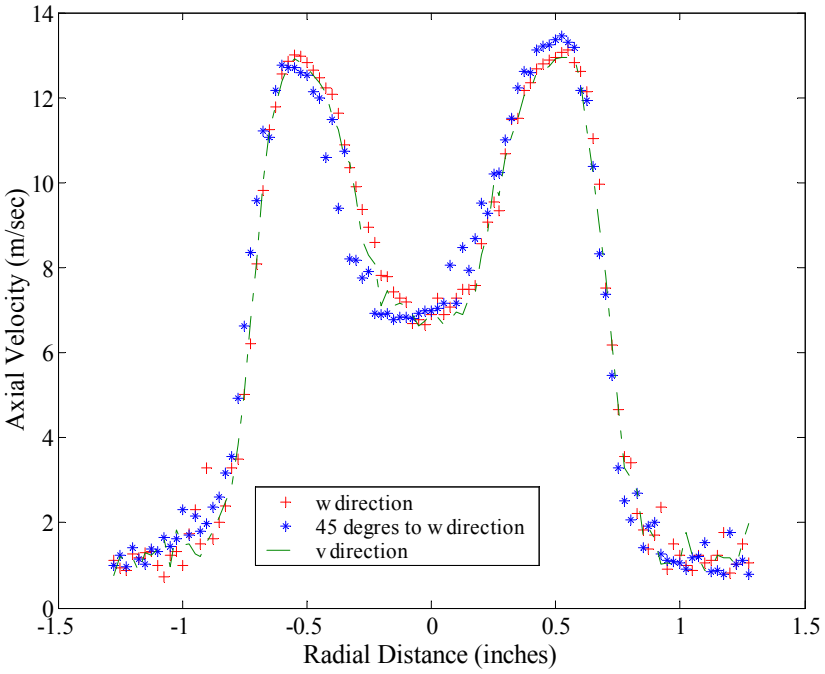


Figure 9.6: Axial Velocity profiles along different diameters measured at 1.5 mm above the inlet of the dump for $Q_{air} = 25$ scfm and $S = 0$

in the '$v$', '$w$' directions and at 45 degrees to '$w$' direction, for a total air flow rate of 25 scfm and no swirl. All the three data sets lie almost on top of each other indicating that the flow field could be considered symmetric and that the center body is properly aligned to the axis of the combustor.

Figure 9.7 and Figure 9.8 respectively show the velocity profiles for three different flow rates and no swirl taken at the inlet of the quarl and at 1.5 mm above the inlet of the dump. Data for the Figure 9.7 was taken at the plane of the quarl inlet that was 2.5 mm above the plane of the center body. Consistent with the expectations, both the figures show a large dip in the velocity in the radial region where the center body is present. The entrance of the dump is 2.5" in diameter, while the inlet of the quarl is 1.5" in diameter. This geometry generates a half cone angle of about 35 degrees over an axial length of $\frac{3}{4}$". Due to such a large cone angle, the jet is expected to separate from the wall as it flows through the quarl. This is evident from the almost zero velocities beyond a radial location of 0.75", seen in Figure 9.8.

Having ensured that the axial jet is well behaved, it was essential to confirm the validity of hotwire data acquired in swirling flows. This is a necessary step, because due to the design and the manufacturing constraints, there are limitations to the maximum effective angle that the total velocity vector can substend to the axis of the hotwire. The maximum effective angle is evaluated using the calibration of the hotwire and if the total velocity vectors generate angles greater than the effective angle with respect to the axis of the flow, the corresponding data lies outside the bounds of calibration and is unreliable. Therefore, data was collected by increasing the swirl from zero to its maximum value by incrementing the percentage split of total air flow that passed through the tangential swirl generator port when compared to the axial air ports. Data was collected at 5 % increments in the flow rate of the tangential air flow from 0 % to 100 %. For each data point collected, the angle subtended by the total velocity vector to the axis of the probe was calculated. All of the calculated angle were less than the effective angle of the probe, thus ensuring that all the data collected could be relied upon. Of all the data collected, only those cases that are relevant to the conditions of the dynamic experiment are shown here. Figure 9.9 through

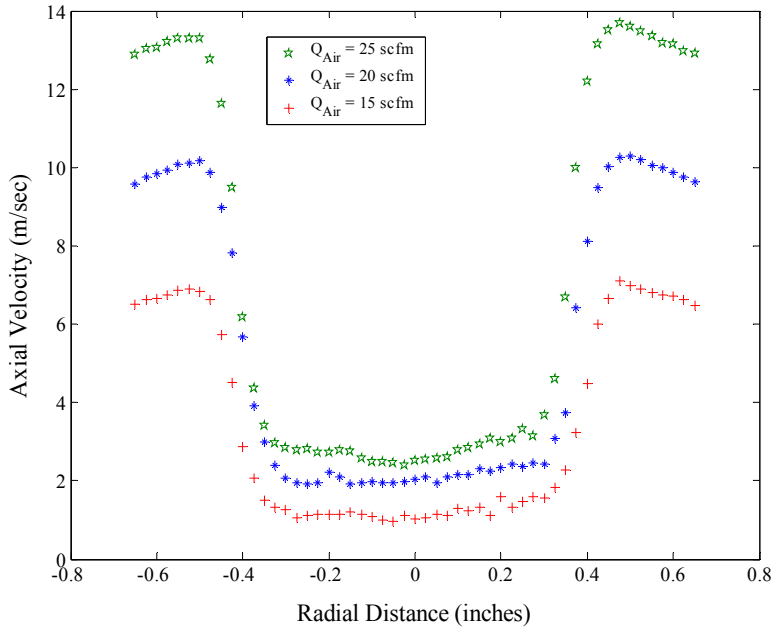


Figure 9.7: Axial Velocity profiles measured at the inlet of the quarl for $S = 0$

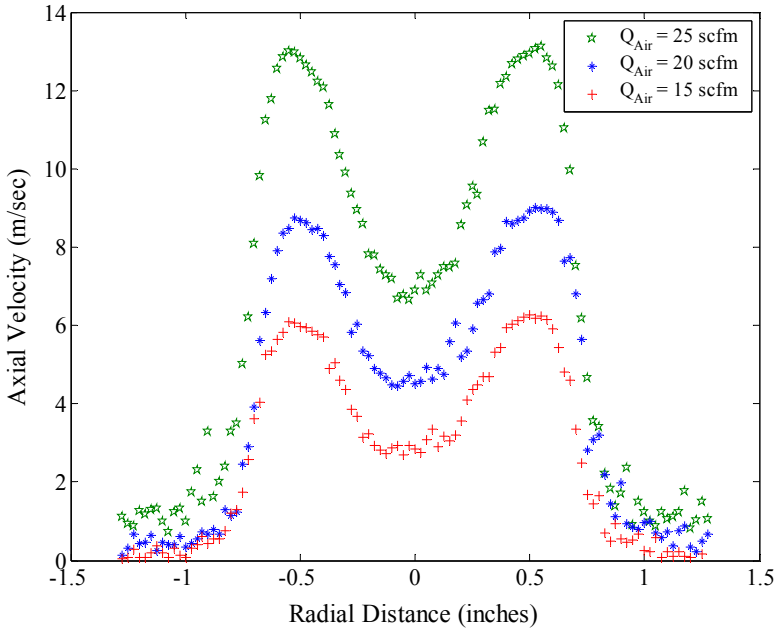


Figure 9.8: Axial Velocity profiles measured at 1.5 mm above the inlet of the dump for $S = 0$

Figure 9.16 show the axial and the tangential velocities measured at $S = 1.19$ and $S = 0.79$ for the three flow rates. Profiles recorded at the inlet of the quarl and at 1.5 mm above the inlet of the dump are presented. The plots indicate that compared to no swirl cases, both the swirl numbers studied ensure that the majority of the flow occurs near the outer bounds of the annulus, thus preventing any flow separation in the quarl. The figures also indicate that an increase in the swirl tends to distort the symmetry of the profiles, especially at the inlet of the quarl. This occurrence is probably due to certain non-uniformities generated while brazing the tangential tubes to the swirl generator. This non-uniformity tends to disappear as the flow passes through the quarl and enters the dump.

## 9.5 Optimization of the Chemiluminescence Measurement

Having characterized the flow field and the acoustics of the combustor, the next step was to ensure the proper functioning of the $OH^*$ chemiluminescence capturing optical system. Based on the optical design and setup described in Chapter 8, Section 8.3.5, the assembly of the optical system was completed. The entire setup was mounted at a distance of 1981 mm from the quartz combustion chamber and at a height of 864 mm above the combustion chamber back plate. The optics was tilted downwards from the horizontal line of sight to be able to view the entire volume of the combustion chamber.

Having mounted the optics, the room was darkened and the flame was lit. 890 volts were applied to the PMT and its current output converted to volts by the current to voltage amplifier was measured. The entire receiving optics and the PMT was moved in the horizontal direction and rotated about the horizontal axis to maximize the output signal. Once the signal maximization was achieved, the position and the orientation of the optics was fixed and was left undisturbed during the entire duration of the data collection.

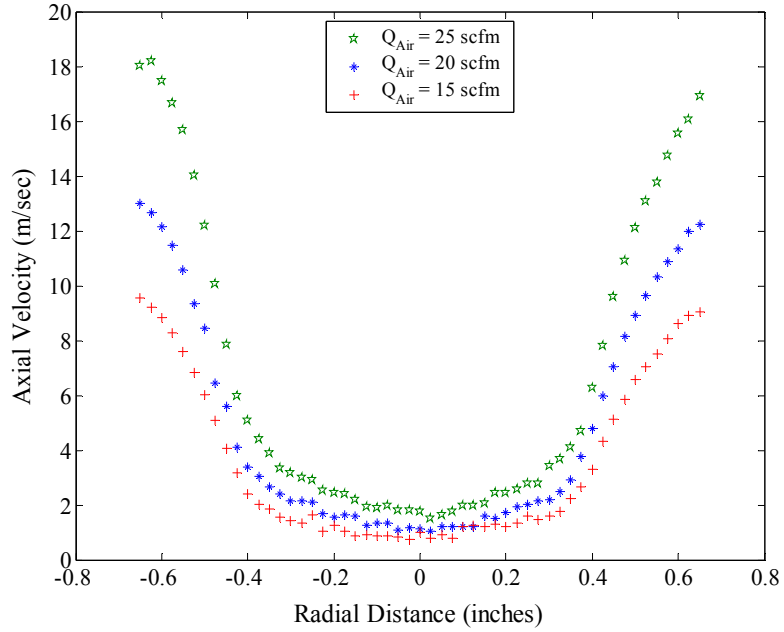


Figure 9.9: Axial velocity profiles measured at the inlet of the quarl for $S = 0.79$

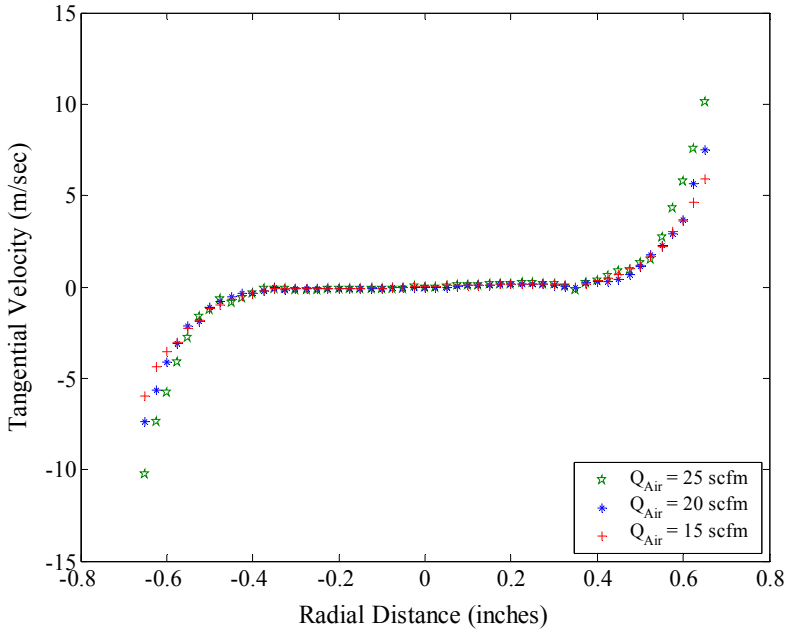


Figure 9.10: Tangential velocity profiles measured at inlet of the quarl for $S = 0.79$

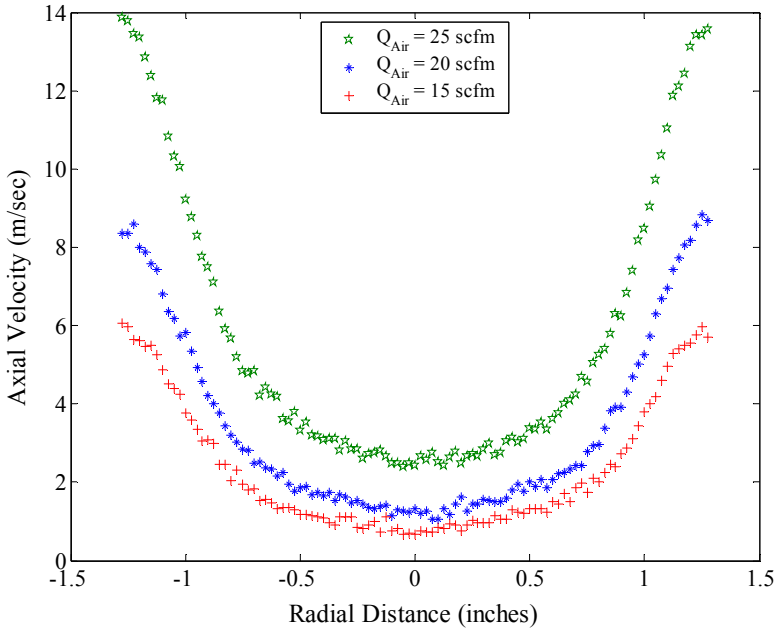


Figure 9.11: Axial velocity profiles measured at 1.5 mm above the inlet of the dump for $S = 0.79$

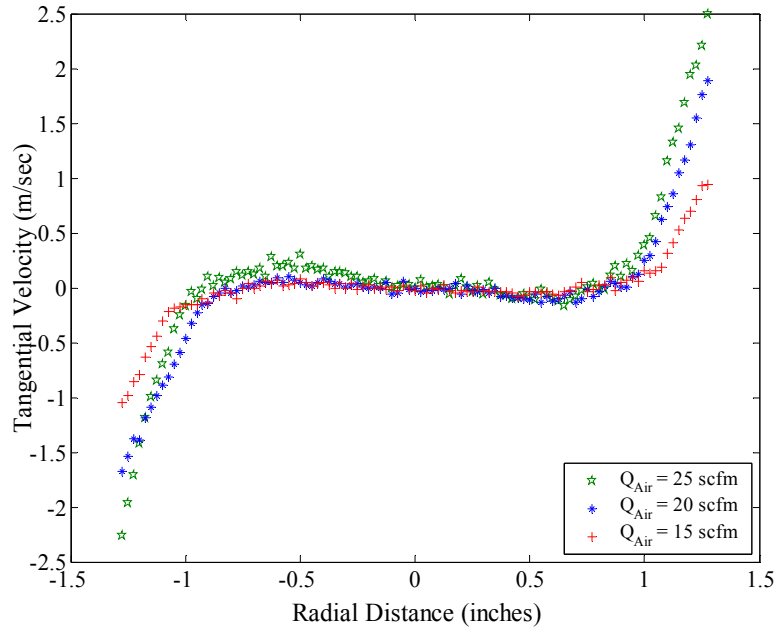


Figure 9.12: Tangential velocity profiles measured at 1.5 mm above the inlet of the dump for $S = 0.79$

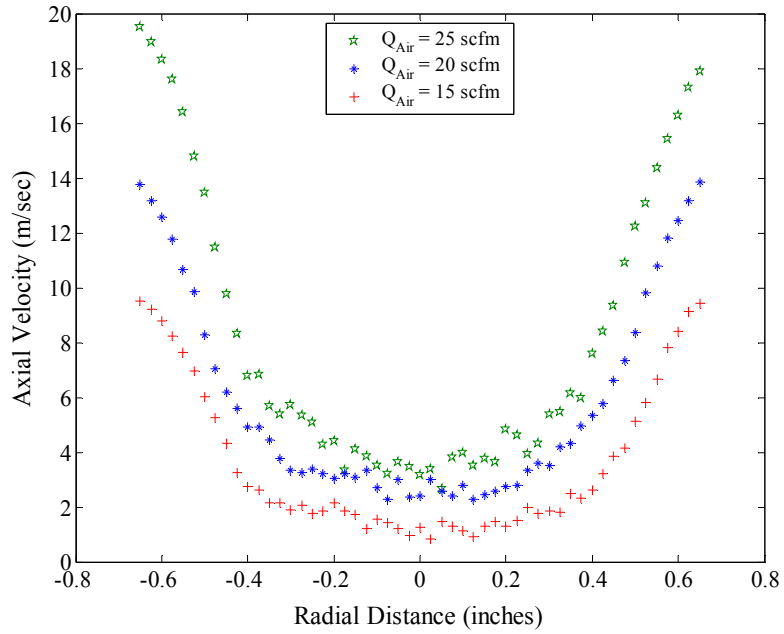


Figure 9.13: Axial velocity profiles measured at the inlet of the quarl for $S = 1.19$

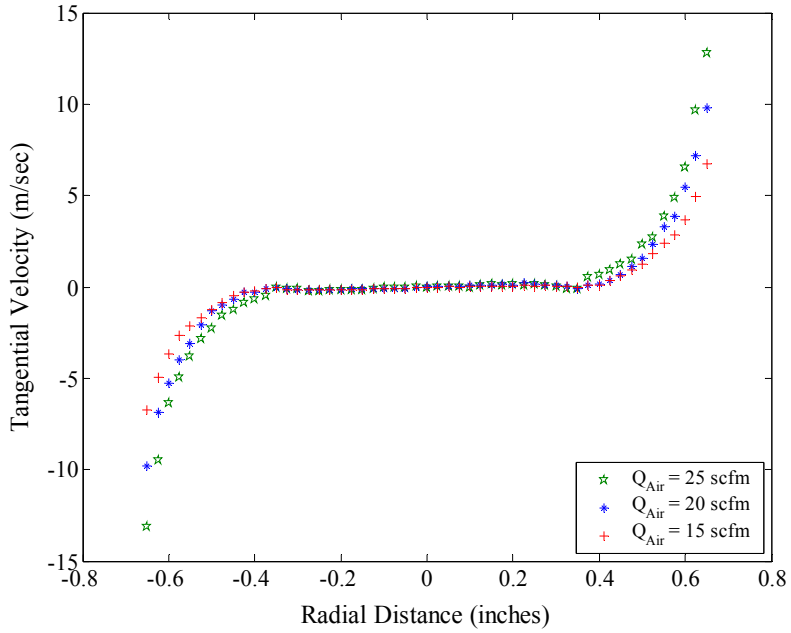


Figure 9.14: Tangential velocity profiles measured at inlet of the quarl for $S = 1.19$

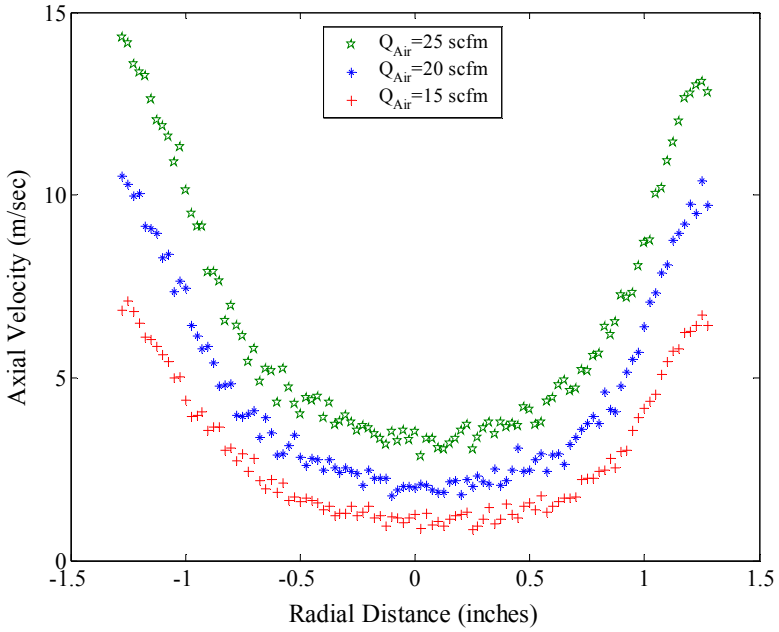


Figure 9.15: Axial velocity profiles measured at 1.5 mm above the inlet of the dump for $S = 1.19$

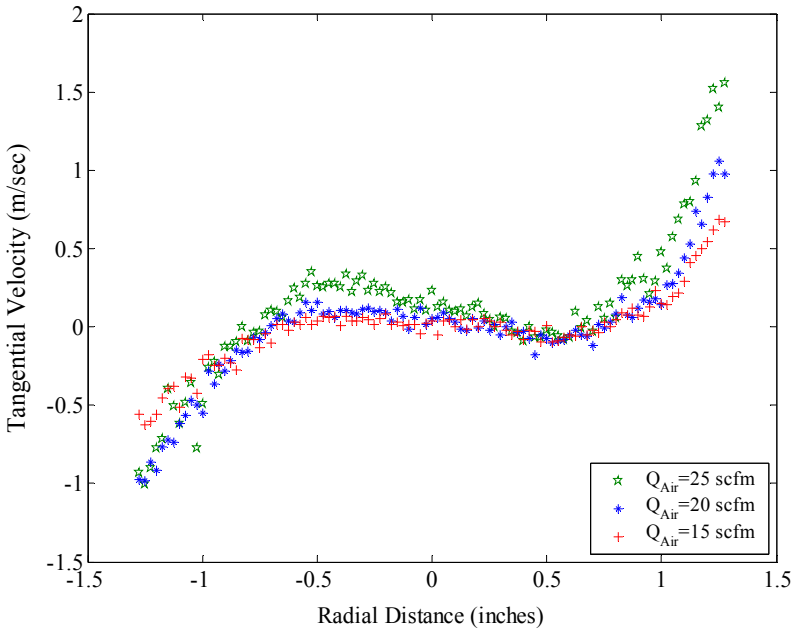


Figure 9.16: Tangential velocity profiles measured at 1.5 mm above the inlet of the dump for $S = 1.19$

## 9.6 Combustor Startup

Prior to running any experiments, it was ensured that all the electronics were in proper working condition. Depending on whether the experiments were conducted in the fully or the partially premixed mode, the various shutoff valves were engaged to alter the flow path. The flow meters were turned on and the flow recordings and the display program were initialized. For the fully premixed cases, the air was measured by the axial mass flow meter and was directed into the mixing chamber. The fuel, after being monitored by the fuel mass flow meter was directed into the mixing chamber, while the flow to the central injection system was cut off. The fully premixed charge of fuel and air from the premixer, was then split into two parts and supplied to the axial and the tangential ports of the combustor. The flow to the tangential port was monitored using the tangential flow meter, while the amount of flow through the axial ports was deduced based on the measurement of the three flow meters and the conservation of mass. For partially premixed conditions, the fuel was supplied to the central fuel injection system. The air flow was split into two branches and supplied to the axial and the tangential ports. Each of the flow streams, the axial air, the tangential air, and the fuel were measured using separate flow meters.

The selected flow paths were pressurized by shutting off the inlets to the combustor and opening the main fuel and the air flow shut off valves. The pressurized flow train was inspected for leaks by applying soap water to all the joints. This important process was religiously carried out to maintain the accuracy of the measured flows and the safety of the work environment. To further ensure the accuracy of the flow data, the zero setting in the flow meters were periodically checked as per the manufacturers instruction manual.

Having ensured the proper functioning of the process control equipment, the air was allowed to flow through the combustor for about 25 minutes. This cleared any unwanted dust in the process system and also stabilized the voltage output of the flow meters. During this period, the flow control valves for the air flow were adjusted to achieve the required flow rate. The room was turned into a dark room, the PMT power supply was turned on and the PMT

output circuit was zeroed. Once the air flow was stabilized and the flow meters had warmed up, the fuel flow was turned on and the flame was lit. The fuel flow rate was then adjusted to achieve the proper equivalence ratio. The flow of cooling water to the center body and the combustion chamber back plate was turned on. The flame was then allowed to stabilize for about 20 minutes, during which the water/ice bath used for the thermocouple measurement was replenished with fresh ice, and the rest of the electronics was turned on. the room was turned into a dark room and the PMT circuit was zeroed. If required, the flow conditions were fine tuned to the desired value once the system and all of the equipment were stabilized.

## 9.7 Data Acquisition Procedure

With the confirmation that all the systems were working satisfactorily, the data acquisition process was initialized. First, the DC values of all the five 'Type R' thermocouples were recorded manually using a voltmeter. Then, the dynamic velocity and the $OH^*$ chemiluminescence signals were processed using the Hewlett Packard frequency analyzer. The power spectrum of the $OH^*$ chemiluminescence under the conditions of no excitation were recorded. The speaker was then imparted a sinusoidal voltage at discrete frequencies starting with 20 Hz. The dynamic velocity and the $OH^*$ chemiluminescence signal were then processed using the frequency analyzer. The magnitude and the phase of the FRF between the two signals along with the coherence and the power spectrum values were recorded at the excitation frequency. Care was also taken to ensure that the coherence was always above 0.9 and that the power spectrum of both the signals did not show any harmonics of the excitation frequency. This was essential to maintain the reliability and the linearity of the response recorded. However, under certain conditions, the power spectrum of the velocity was allowed to exhibit harmonics that were 25 dBV below the fundamental frequency, but under no circumstances was the $OH^*$ signal allowed to exhibit any harmonics of the excitation frequency.

Once satisfactory data at a particular excitation frequency was measured, the excitation frequency was incremented to the next value and the process was repeated. Between 20 Hz

and 85 Hz, data was collected at increments of 2.5 Hz. Beyond 85 Hz, a 5 Hz increment was used to determine the next excitation frequency. The last frequency for which the data was collected varied based on the ability to obtain satisfactory and reliable data. However for some cases, the data collection range was from 20 to 490 Hz. The manually recorded data was fed into a text file that was processed using codes written in Matlab.